Original Articles

Acupuncture and Herbal Medicine

OPEN

Construction of curcumin-loaded micelles and evaluation of the anti-tumor effect based on angiogenesis

Rui Liu[1,2,3], Zhongyan Liu[1,2,3], Xueli Guo[1,2,3], Dereje Kebebe[4,*], Jiaxin Pi[1,2,3,*], Pan Guo[1,2,3,*]

Abstract

Objective: Inhibition of tumor angiogenesis has become a new targeted tumor therapy. In this study, we established a micellar carrier with a tumor neovascularization-targeting effect modified by the neovascularization-targeting peptide NGR.

Methods: The targeted polymer poly(ethylene glycol)-b-poly(lactide-co-glycolide) (PEG-PLGA) modified with Asn–Gly–Arg (NGR) peptide was prepared and characterized by ^{1}H nuclear magnetic resonance and Fourier-transform infrared spectrometry. NGR-PEG-PLGA was used to construct curcumin (Cur)-loaded micelles by the solvent evaporation method. The physicochemical properties of the micelles were also investigated. Additionally, we evaluated the antitumor efficacy of the polymer micelles (PM) using *in vitro* cytology experiments and *in vivo* animal studies.

Results: The particle size of Cur-NGR-PM was 139.70 ± 2.51 nm, and the drug-loading capacity was 14.37 ± 0.06%. *In vitro* cytological evaluation showed that NGR-modified micelles showed higher cellular uptake through receptor-mediated endocytosis pathways than did unmodified micelles, leading to the apoptosis of tumor cells. Then, *in vivo* antitumor experiments showed that the modified micelles significantly inhibited tumor growth and were safe.

Conclusions: NGR-modified micelles significantly optimized the therapeutic efficacy of Cur. This strategy offers a viable avenue for cancer treatment.

Keywords: Antitumor therapy, Curcumin (Cur), Micelles, NGR, Tumor angiogenesis

Graphical abstract: http://links.lww.com/AHM/A69.

Introduction

Angiogenesis occurs under physiological and pathological conditions. Notably, tumors develop following excessive angiogenesis. During tumor growth and migration, many new blood vessels are formed, providing nutrients and water and transporting metabolites to meet the needs for tumor growth. Angiogenesis is closely related to tumor growth and metastasis and plays a vital role in tumor development and progression. Therefore, anti-angiogenesis is a feasible treatment strategy for tumors[1]. Anti-angiogenic therapy can stop tumor growth and spread by inhibiting angiogenesis around the tumors. It is achieved by inhibiting the production or action of angiogenic factors, thereby preventing the formation of new blood vessels. Simultaneously, this therapy can destroy the existing abnormal capillary network, causing the tumor to lose its nutrients and oxygen supply, thereby slowing or stopping tumor growth. Currently, targeted treatment of cancer using tumor site overexpression factors is considered to be an effective treatment strategy.

Aminopeptidase N (APN/CD13), a marker of the neovascular system, has high expression in neovascular endothelial cells and some tumor cells and low expression in normal vascular endothelial cells[2–3]; specifically, it plays an important role in forming new blood vessels and the growth and metastasis of tumors. High expression of APN in tumor cells is closely related to various biological behaviors, such as proliferation, invasion, metastasis, and drug resistance of tumor cells. APNs can also promote tumor cell invasion and metastasis by regulating mechanisms such as the degradation of the extracellular matrix and cell-to-cell signaling. Therefore, APN/CD13 is an important target for tumor treatment and neovascular imaging. Recent studies have shown that APNs are members of a family of surface markers of liver cancer stem cells. Therefore,

[1] *State Key Laboratory of Component-Based Chinese Medicine, Tianjin University of Traditional Chinese Medicine, Tianjin, China;* [2] *Engineering Research Center of Modern Chinese Medicine Discovery and Preparation Technique, Ministry of Education, Tianjin, China;* [3] *Haihe Laboratory of Modern Chinese Medicine, Tianjin, China;* [4] *School of Pharmacy, Institute of Health, Jimma University, Jimma, Ethiopia*

**Corresponding author. Dereje Kebebe, School of Pharmacy, Institute of Health, Jimma University, Jimma, Ethiopia, E-mail: dereje.keborg@gmail.com; Jiaxin Pi, State Key Laboratory of Component-Based Chinese Medicine, Tianjin University of Traditional Chinese Medicine, Tianjin 301617, China, E-mail:ppstar9999@sina.com; Pan Guo, State Key Laboratory of Component-Based Chinese Medicine, Tianjin University of Traditional Chinese Medicine, Tianjin 301617, China, E-mail: gpandap@163.com*

Acupuncture and Herbal Medicine (2023) 3:4

Received 4 May 2023 / Accepted 18 September 2023

http://dx.doi.org/10.1097/HM9.0000000000000079

small-molecule APN inhibitors may have multiple complex functions and exert multiple antitumor effects on cancer development and staging. Notably, CD13 has various biological functions. (1) CD13 is expressed on the surface of endothelial cells, monocytes, and other cells, participates in the enzymatic lysis of polypeptide chains, and regulates various intracellular signal transduction processes as signaling molecules, including cell migration, viral uptake, and vascularization[4]. (2) Furthermore, CD13 is expressed at high levels on the surface of tumor cells such as breast, ovarian, and prostate cancer cells and degrades the extracellular matrix by hydrolyzing proteases to promote tumor invasion and metastasis[5–6]. (3) Specifically, CD13 fosters neovascularization in tumor tissues through its particular expression in vascular endothelial and subendothelial cells and can promote the deterioration and metastasis of tumor cells by degrading thymus peptides and interleukins and the proliferation of liver cancer cells by accelerating the liver cancer cell cycle. Therefore, researchers believe that CD13, a crucial tumor-associated antigen, could become an essential target for tumor treatment.

Curcumin (Cur) is a natural polyphenolic component with various pharmacological effects such as anti-oxidation, anti-inflammation, infection prevention, liver prevention, and cardiovascular disease prevention[7]. Among these, anti-tumor effects are the most prominent[8–10]. Cur exerts its anti-tumor effects through multiple mechanisms, including inhibiting the expression of oncogenes[10], inducing tumor cell apoptosis[11], inhibiting tumor angiogenesis[12], increasing the sensitivity of tumor cells to chemotherapy[13], and inducing oxidative damage[14]. Recently, much attention has been paid to Cur as an anti-angiogenic agent, the potential anti-angiogenic effect of which has become an attractive drug target in cancer therapy.

However, the instability, poor water solubility, low absorption rate, and fast metabolism of Cur hinder further development of its therapeutic potential[15]. The application of nanotechnology and nanocarriers provides a solution that can potentially target specific sites for drug release and can be used in anti-angiogenic therapy. In addition, encapsulating Cur in tumor-targeting micelles can increase its solubility, increase blood circulation time, improve stability, and enhance anti-tumor effects.

Poly(ethylene glycol)-b-poly(lactide-co-glycolide) (PEG-PLGA) has good biodegradability and biocompatibility. Both PEG and PLGA have been approved by the Food and Drug Administration[16]. These advantages make PEG-PLGA an ideal vehicle for micellar formulations. Moreover, peptides containing asparagine–glycine–arginine (Asn–Gly–Arg) sequences specifically bind to CD13 receptors and exert precise targeting effects[17]. The CD13 subtype, recognized by NGR peptides, is a unique molecular marker for cancer therapy. Therefore, NGR can be used to modify the surface of PEG-PLGA to form micelles with tumor neovascularization-targeting effects.

In order to target tumor blood vessels, we designed and constructed a micellar carrier system. This study modified polypeptides at the hydrophilic end of PEG-PLGA (NGR-PEG-PLGA). Cur-loaded polymeric micelles (Cur-NGR-PM) were prepared and characterized. The anti-tumor activities of the Cur micelles were investigated *in vitro* and *in vivo*. The cytotoxicity and cellular uptake of Cur-NGR-PM were also studied in detail. Subsequently, *in vivo* distribution of Cur micelles was studied. Additionally, subcutaneous H22 xenograft mouse models were established and used to evaluate the antitumor activity of Cur-NGR-PM. Our findings indicated that Cur-NGR-PM showed improved anti-angiogenesis and anti-tumor activity both *in vitro* and *in vivo* and may have potential applications in hepatic carcinoma therapy.

Materials and methods

Materials and animals

DL-lactide-co-glycolide (PLGA, 75/25 Poly, MW 20 kDa; mPEG, MW 5 kDa) was purchased from Daigang Biological Science and Technology Co., Ltd. (Shandong, China). The Asn–Gly–Arg (NGR) peptide was obtained from Xi'an Ruixi Biological Technology (Xi'an, China). Curcumin (batch number: R30A11S112330, purity: 95%) was obtained from Shanghai Yuan Ye Biological Technology Co., Ltd. (Shanghai, China). N-hydroxysuccinimide (NHS) (batch number: F1829107, purity 98%) and 1-(3-dimethylaminopropyl)-3-ethylcarbodiimide hydrochloride (EDC) (batch number: G1806067, purity 98%) were purchased from Aladdin Industries Inc. (Nashville, TN, USA). Serum alanine aminotransferase (ALT), aspartate aminotransferase (AST), and creatinine (CRE) levels were determined from the Institute of Bioengineering (Nanjing, China). Hematoxylin was obtained from Wuhan Biotechnology Co., Ltd. (China). 3-(4,5)-dimethylthiahiazo (-z-y1)-3,5-di- phenytetrazoliumromide (MTT) was purchased from Solarbio (Beijing, China). Sephadex G-50 was purchased from Beijing Solarbio Biotechnology Co. Ltd. (Beijing, China). All the other reagents were of analytical grade.

HepG2 cells were kindly provided by the Cell Bank, Chinese Academy of Sciences (Shanghai, China) and were grown in Dulbecco's Modified Eagle Medium (DMEM) supplemented with 10% fetal bovine serum (FBS), HEPES (25 mM), $NaHCO_3$ (3.7 g/L), penicillin (100 U/mL), and streptomycin (100 g/mL). H22 cells were obtained from the Institute of Basic Medical Sciences of the Chinese Academy of Medical Sciences (Beijing, China). H22 cells were grown in HyClone RPMI 1640 medium containing 10% FBS, 100 U/mL penicillin, and 100 g/mL streptomycin. EA.hy926 cells were obtained from Wuhan Shang En Biotechnology Co., Ltd. (Wuhan, China) and grown in DMEM supplemented with 10% FBS, HEPES (25 mM), $NaHCO_3$ (3.7 g/L), penicillin (100 U/mL), and streptomycin (100 g/mL). All the cells were incubated in a humidified incubator containing 5% CO_2 and 95% air in an incubator at 37°C. Cells were maintained in the logarithmic growth phase by routine passaging every 3 days.

Male BALB/c mice (Vital River Laboratory Animal Technology, Beijing, China), weighing 18 to 20 g, were acclimated at 25°C and 55% of humidity under

natural light/dark conditions for 1 week before the study, with free access to standard food and water. All animal care and handling were performed with the approval of Tianjin University of Traditional Chinese Medicine (License: TCM-LAEC2022128, Tianjin, China).

Synthesis and characterizations of NGR-PEG-PLGA

NGR-PEG-PLGA was prepared according to a previously reported method[18–20]. Briefly, NGR was conjugated to PEG-PLGA using NHS. NHS was added to PEG-PLGA to activate the carboxyl groups in N,N-Dimethylformamide (DMF) at a molar ratio of 1:1 (NHS: PEG-PLGA). Moreover, NGR was added to modify the peptide using NHS-PEG-PLGA at a molar ratio of 1:2. The reaction mixture was maintained at room temperature for 24 hours with moderate stirring. The final solution was placed in a dialysis bag with a molecular weight cutoff of 3,500 Da dialysis bag and dialyzed against deionized water for 48 hours to remove unconjugated NGR and other impurities. Finally, lyophilized and stored at –20°C until use. Thus, NGR-PEG-PLGA was obtained and used for further analysis.

Fourier-transform infrared spectrometry (FTIR) uses the chemical bonds in molecules to absorb infrared light and determine the structure of the synthesized polymers. ^{1}H nuclear magnetic resonance (^{1}H NMR) techniques use NMR signals from hydrogen atoms to determine the chemical bonds in the synthesized polymers and their environment. Spectra were recorded using a 600-MHz JEOL spectrometer (^{1}H NMR, JNM-ECZ600R, Tokyo, Japan) at 25°C. Deuterated chloroform ($CDCl_3$) was used as the solvent. The functional groups were characterized by FTIR spectroscopy (Thermo Nicolet, Massachusetts, USA). The samples were prepared by spreading NGR-PEG-PLGA onto a potassium bromide tablet.

Preparation of the Cur-loaded PM

Cur-loaded NGR-PEG-PLGA micelles were prepared using a solvent evaporation method[21–22]. In brief, Cur and NGR-PEG-PLGA were dissolved in acetonitrile. A small amount of Cremophor EL 35 was added to the aqueous phase as a surfactant. The organic phase was dripped into deionized water and stirred continuously at high speed. When acetonitrile had completely evaporated, the suspension was filtered by Sephadex G-50 microcolumn centrifugation to eliminate unloaded Cur. The filtrate was collected to obtain Cur-loaded PM and labeled Cur-NGR-PM. Blank NGR-PM and unmodified Cur-PM micelles were prepared similarly.

Morphology, particle size, and zeta potential

Dynamic laser scattering technology (Malvern Instruments, Worcestershire, UK) was used to determine the particle size and potential detection of formulations. Transmission electron microscopy (TEM; JEM-1200EX, JEOL, Tokyo, Japan) was used to analyze the topography of the micelles.

Determination of encapsulating efficiency and loading capacity

The entrapment efficiency of Cur by different PM types was assessed using high-performance liquid chromatography (HPLC). As reported in the literature, improved size-exclusion chromatography was used to separate free drugs and micelles[22–23]. Briefly, Sephadex G-50 was wet-packed with columns. Sample was added to the top of the microcolumn, centrifuged at 1500 rpm, and eluted. Micelles and free drugs were separated according to their molecular size, and the lower micelles were collected. HPLC was used to determine drug concentration after demulsification. The drug-loading efficiency and drug encapsulation efficacy were calculated using the following formulae:

$$\text{Encapsulation efficiency (EE)} = \frac{\text{Wa}}{\text{Wb}} \times 100\ \%$$

$$\text{Drug loading efficiency (DE)} = \frac{\text{Wa}}{\text{Wc}} \times 100\ \%,$$

where Wa, Wb, and Wc are the drug weights in the micelles, initial drug, and micelles, respectively.

Quantitative determination of Cur was performed using HPLC (Agient 1260; Agilent Technologies, California, USA).

In vitro drug-release profile study

Dialysis is commonly used for evaluating *in vitro* drug release[24]. Briefly, a 2 mL (0.8 mg Cur) sample was transferred into a dialysis bag (molecular weight cutoff 8,000 Da). Next, the dialysis bag was placed into a 50 mL phosphate buffer solution (pH 7.4, 0.5% w/v Tween 80) release medium and placed on a constant temperature shaker at 37°C to study the drug-release profile. At predetermined time intervals (0, 0.17, 0.5, 1, 2, 3, 4, 6, 8, 10, 12, 24, 36, 48, 60, and 72 hours), 1 mL of each sample was added to an equal volume of fresh phosphate buffer solution. After the experiment, the amount of Cur released was evaluated using HPLC.

Differential scanning calorimetry

The form of Cur in the different formulations (Cur, NGR-PM, physical mixture of Cur and PEG-PLGA, Cur-PM, and Cur-NGR-PM) was investigated by differential scanning calorimetry (DSC). DSC measurements were conducted using a thermal analyzer (DSC822e; Mettler Toledo GmbH, Greifensee, Switzerland). The samples were heated from 100°C to 250°C at a constant heating rate of 20°C/min under a 50 mL/min nitrogen flow.

In vitro cytotoxicity and cellular uptake

The MTT method is commonly used to evaluate cytotoxicity, and quantitative results can be obtained by evaluating the cytotoxicity of PM using the MTT assay, which can be used to compare the toxicity differences of different PMs and provide a reference for the toxicity evaluation of PM. HepG2 and EA.hy926 cells were cultured in 96-well plates. Cells were cultured at a density of 10^4 per well for 24 hours with 100 µL of medium per well.

The cells were subsequently treated with various concentrations (2, 5, 10, 15, 20, and 30 μg/mL, Cur equiv.) of PMs (Cur-Sol, NGR-PM, Cur-PM, and Cur-NGR-PM) for 24 hours at 37°C. After cultivation, the cells were treated with 20 μL of the MTT solution (5 mg/mL) for 4 hours. The culture medium was subsequently discarded, and 150 μL of dimethyl sulfoxide was added to dissolve the formazan crystals. The absorbance of each well was measured at 490 nm after gentle shaking for 10 minutes. Data were expressed as the percentage of viable cells relative to the survival of the control group (untreated cells were used as controls, with a survival rate of 100%).

$$\text{Cell viability rate } (\%) = \left(\frac{\text{As} - \text{Ab}}{\text{Ac} - \text{Ab}}\right) \times 100\ \%,$$

where Ac, As, and Ab refer to the control wells, experimental wells, and the absorbance of the blank wells, respectively.

High-content analysis (HCA) and flow cytometry (FCM) are common techniques for analyzing cellular uptake. Coumarin 6 (Cou6) exhibits green fluorescence and is typically used to examine cellular uptake[25]. HepG2 cells were seeded at a density of 8×10^3 per well in 96-well plates and incubated at 37°C. After 24 hours, the medium was replaced with a culture medium containing different micelle materials. The final micelle concentration was 0.03 μg/mL (Cou6-equiv.). The dosing time point was set to 2, 4, and 6 hours after administration, and to investigate the drug uptake by cells during these times, the sample was placed in an incubator at 37°C. After incubation, the nuclei were stained with 50 μL (15 μg/mL) of Hoechst solution in each well and incubated at 37°C for 30 minutes. Subsequently, the liquid in the wells was aspirated, uptake was terminated, and the cells were washed twice with phosphate-buffered saline (PBS) to remove the fluorescent floating color. A 96-well plate was placed in an HCA (GE Healthcare, Illinois, USA) for qualitative and quantitative intake analyses.

A quantitative study of the cellular uptake of micelles was performed using FCM. HepG2 cells were seeded in a 6-well plate at 1×10^5 cells/well density and incubated for 24 hours. The culture medium was then replaced with fresh medium containing 0.05 μg/mL of Cou6-Sol, Cou6-PM, and Cou6-NGR-PM and incubated at 37°C for 2, 4, and 6 hours, respectively. The cells were then washed thrice with PBS, digested with 0.25% trypsin-EDTA, and centrifuged. The precipitate was resuspended in 500 μL of PBS and assayed by FCM (EPICSXL, Beckman, California, USA).

In vivo bio-distribution study

Real-time near-infrared fluorescence imaging (NIRF) is a noninvasive imaging technique that can be used to study drug distribution *in vivo*. To explore the liver-targeting properties of the NGR-modified PM, tumor-bearing mice were subcutaneously injected with H22 cells. Briefly, an appropriate number of H22 cells was injected into the subcutaneous tissue of mice to form tumors. The mice were randomly divided into four groups: saline, Dir-Sol, Dir-PM, and Dir-NGR-PM ($n = 3$). The tumor volume of the mice was increased to 200 mm^3 (tumor volume: $V = ab^2/2$, where a is the tumor length and b is the tumor width). The different formulations were administered at a dose of 0.5 mg/kg of Dir. At 1, 4, 12, and 24 hours after administration, the mice were anesthetized and placed in an In Vivo Imaging System (IVIS) to observe fluorescence intensity at excitation and emission wavelengths of 710 and 800 nm, respectively. Each group was sacrificed, the heart, lungs, liver, spleen, kidneys, and tumors were collected, and their fluorescence intensities were measured.

In vivo anti-tumor effect

This study investigated the antitumor efficacy of H22 tumor cells[26]. The mouse model modeling method was the same as described earlier. Tumor-bearing mice were randomly divided into six groups of six mice each: saline, Cur-Sol, NGR-PM, Cur-PM, and Cur-NGR-PM. Each mouse was intravenously administered the corresponding formulation. Each mouse was injected with 0.2 mL of the formulations, with Cur at 10 mg/kg. The mice were administered the same treatment every 2 days, and their weight and tumor growth were monitored. Tumor volume was measured using a caliper every 2 days for 12 days. All animals were euthanized after the experiments. The organs and tumors were harvested and weighed. Harvested organs were fixed in formalin and embedded in paraffin for hematoxylin and eosin (H&E) staining. The harvested tumors were fixed in a formalin solution to prevent decay and maintain cell structure. The sections were then embedded in paraffin for immunohistochemical analysis.

The inhibition rate of body weight (IRBW), tumor volume, tumor inhibition ratio (TIR), and tumor growth inhibition (TGI) are significant indicators of antitumor efficacy *in vivo* and were calculated using the following formulas:

$$\text{IRBW } (\%) = \left(1 - \frac{\text{BWa}}{\text{BWb}}\right) \times 100\ \%$$

$$\text{TIR } (\%) = \left(\frac{\text{Wo} - \text{Wi}}{\text{Wo}}\right) \times 100\ \%$$

$$\text{TGI } (\%) = \left(1 - \frac{\text{T} - \text{To}}{\text{C} - \text{Co}}\right) \times 100\ \%,$$

where BWa and BWb indicate the body weights of mice before and after treatment, respectively. Furthermore, Wo and Wi are the tumor weights in the control and treatment groups, respectively, and T and To are the average tumor volumes in the treatment group on the last day of treatment and before treatment, respectively. Lastly, C and Co are the average tumor volumes before and after treatment in the control group, respectively.

A standard assay kit (Jiancheng Bioengineering, Nanjing, China) was used to determine the levels of serum liver injury markers (ALT, AST, and CRE) in the different animal groups.

Determination of microvascular density in tumor tissue

CD31 staining is a commonly used immunohistochemical technique to detect tumor tissue microvascular density (MVD). This method uses CD31 antibodies to bind to the CD31 protein on the surface of endothelial cells in the tumor tissue, thereby marking microvessels

in the tumor tissue. Briefly, tumor tissue specimens were subjected to paraffin sectioning. The sections were dewaxed, and antigen retrieval was performed to enable proteins in the tissue to bind to antibodies. CD31 antibodies were then added to bind to the CD31 protein in the tumor tissue. A secondary antibody that binds to the CD31 antibody to form a complex was added. Finally, chromogen was added to make the complex colorless. The sections were observed under a microscope, and the density of the microvessels in the tumor tissue was calculated.

Statistical analysis

The data obtained were expressed as the mean ± standard deviation. SPSS (version 26.0) was used for the data analysis. Analysis of variance and Student *t* test were used to evaluate statistical significance. Differences were considered statistically significant at $P < 0.05$, $P < 0.01$, or $P < 0.001$.

Results

Synthesis and characterization of NGR-PEG-PLGA

The ^{1}H NMR spectra of PEG-PLGA, NGR, and NGR-PEG-PLGA are shown in Figure 1A–C, respectively. The peaks at d (ppm) 1.6 represent the methyl protons (-CH_3) in PLGA, the peak at d (ppm) 4.8 represents the methylene protons (-CH_2-) in the branching units of PLGA, the peak at d (ppm) 5.2 represents the hypomethyl protons (-CH-) in PLGA, and the peak at d (ppm) 3.6 represents the methylene protons (-CH_2-) in PEG[27], demonstrating the structure of PEG-PLGA (Figure 1A). The successful synthesis of NGR-PEG-PLGA was confirmed by the appearance of signals at 2.7 to 3.0 ppm and 1.4 to 2.7 ppm corresponding to the characteristic peaks of NGR (Figure 1B)[28]. The peak in the NGR-PEG-PLGA spectrum at 4.3 ppm represents a proton in the amide bond (-CO-NH-) (Figure 1C).

The infrared spectra of PEG-PLGA, NGR, and NGR-PEG-PLGA are shown in Figure 2. The peaks at 1,452.31 and 1,382 cm^{-1}, similar to the methyl peaks in PEG-PLGA, were assigned to the characteristic polymer methyl groups. The peaks at 2,878 and 1,082 cm^{-1} show the characteristics of the methylene group of the polymer near an oxygen atom and the C-O-C group, respectively, demonstrating the presence of an ether linkage of PEG in the polymer. The peak at 1,747 cm^{-1}, similar to the site of the carbonyl group in PEG-PLGA, represents the carbonyl group in the polymer, while the peak at 1,180 cm^{-1} represents the C-O linkage of the ester in the polymer. These groups comprise the original functional groups of PEG-PLGA. Moreover, the peaks at 3,750 to 3,000 cm^{-1} show the characteristics of the NH groups[27], which were attributed to the amine group of NGR.

These results confirm the successful synthesis of NGR-PEG-PLGA by coupling PEG-PLGA with NGR *via* amide bonds. The polymer was self-assembled into micelles in the aqueous phase. The internal hydrophobic group was used to load Cur, and the NGR peptide linked to the hydrophilic group delivered the micelles to the tumor neovascularization site by specifically binding to the CD13 receptor.

Preparation of Cur-loaded PM and characterization

This study successfully prepared PM encapsulated in Cur by solvent volatilization as previously described[21–22]. The PM was characterized using a Zetasizer system (Malvern NanoZS, Worcestershire, UK). The average particle size of Cur-PM was 150 nm, with a polydispersity index (PDI) of 0.2 and a mean zeta potential <–10 mV (Table 1, Figure 3A, B). Furthermore, Cur-PM exhibited a uniform, near-spherical morphology in TEM images (Figure 3C).

All encapsulation efficiency (EE) results were above 80%, indicating that PM has a good encapsulation ability for Cur, possibly due to its high lipid solubility. There were no significant differences in the DE and EE between the modified Cur-PM and unmodified Cur-PM, indicating that surface modification did not affect the EE and DE of the PM.

The structure of the PEG-PLGA copolymers was an A-B diblock-type. PEG is a representative hydrophilic segment, whereas PLGA is a hydrophobic one. PEG-PLGA copolymers initially existed as monomers at concentrations below the CAC. As the concentration of the polymers increases to or exceeds the CAC, they undergo self-assembly to aggregate as a micellar system[29]. This self-assembly process is due to changes in the PEG and PLGA molecules' interaction force, resulting in polymer molecule aggregation.

In PEG-PLGA micelles, PLGA is hydrophobic and forms a hydrophobic nucleus, whereas PEG is hydrophilic and forms a hydrophilic shell. This core-shell structure

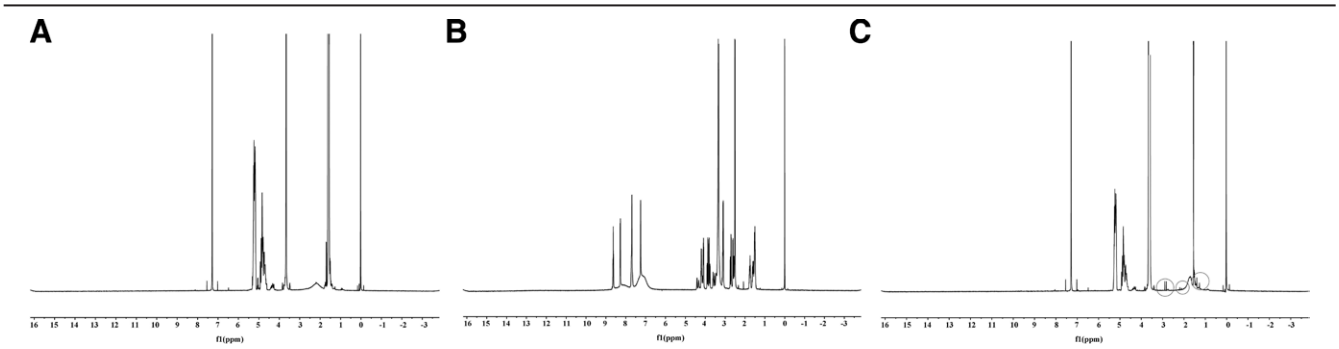

Figure 1. ^{1}H NMR spectra of PEG-PLGA (A), NGR (B), and NGR-PEG-PLGA(C) in $CDCl_3$. $CDCl_3$: Deuterated chloroform; ^{1}H NMR: ^{1}H nuclear magnetic resonance; NGR: Asn–Gly–Arg; PEG-PLGA: Poly(ethylene glycol)-b-poly(lactide-co-glycolide).

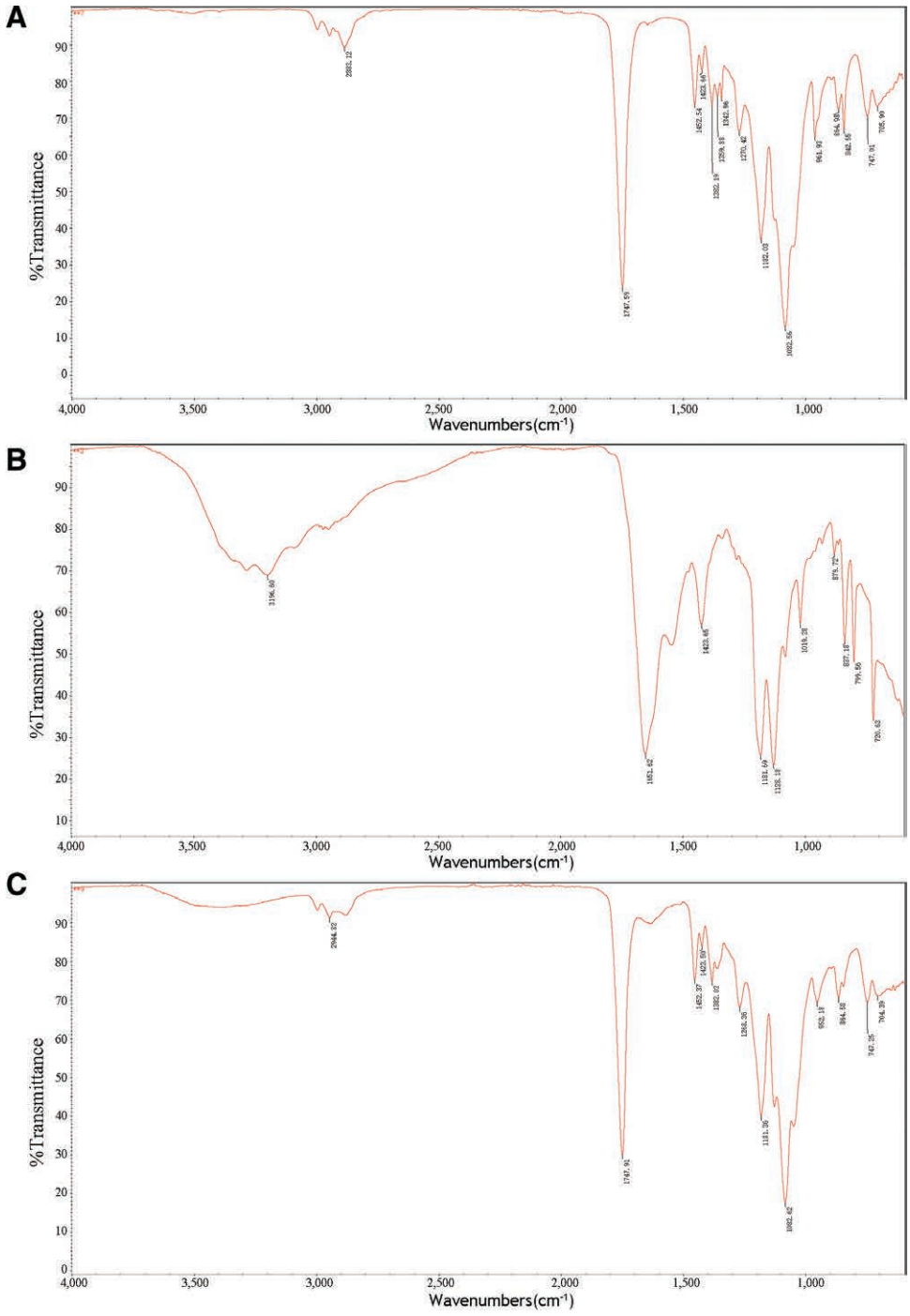

Figure 2. IR spectrum of PEG-PLGA (A), NGR (B), and Cur-PEG-PLGA (C). Cur: Curcumin; IR: Infrared Radiation; NGR: Asn–Gly–Arg; PEG-PLGA: Poly(ethylene glycol)-b-poly(lactide-co-glycolide).

Table 1.

Physicochemical characteristics of NGR-PM, Cur-PM, and Cur-NGR-PM (mean ± SD, *n* = 3)

Preparation	Size (nm)	PDI	Zeta potential (mV)	EE (%)	DE (%)
NGR-PM	116.67 ± 0.21	0.21 ± 0.01	−12.30 ± 0.14	–	–
Cur-PM	151.77 ± 1.63	0.22 ± 0.01	−12.60 ± 0.62	81.30 ± 3.53	13.55 ± 0.67
Cur-NGR-PM	139.70 ± 2.51	0.19 ± 0.01	−15.57 ± 0.25	86.40 ± 0.26	14.37 ± 0.06

Cur: Curcumin; DE: Drug encapsulation efficiency; EE: Encapsulation efficiency; NGR: Asn–Gly–Arg; PDI: Polydispersity index; PM: Polymer micelles; SD: Standard deviation.

makes PEG-PLGA micelles biocompatible and biodegradable; therefore, they are widely used in drug delivery systems. In addition, PEG-PLGA micelles can achieve targeted delivery through surface modification, such as the covalent binding of targeted molecules (such as antibodies, peptides, and sugars) to the surface of PEG-PLGA micelles. Targeted delivery can increase the local concentration of the drug, reduce its side effects, and improve its therapeutic effect.

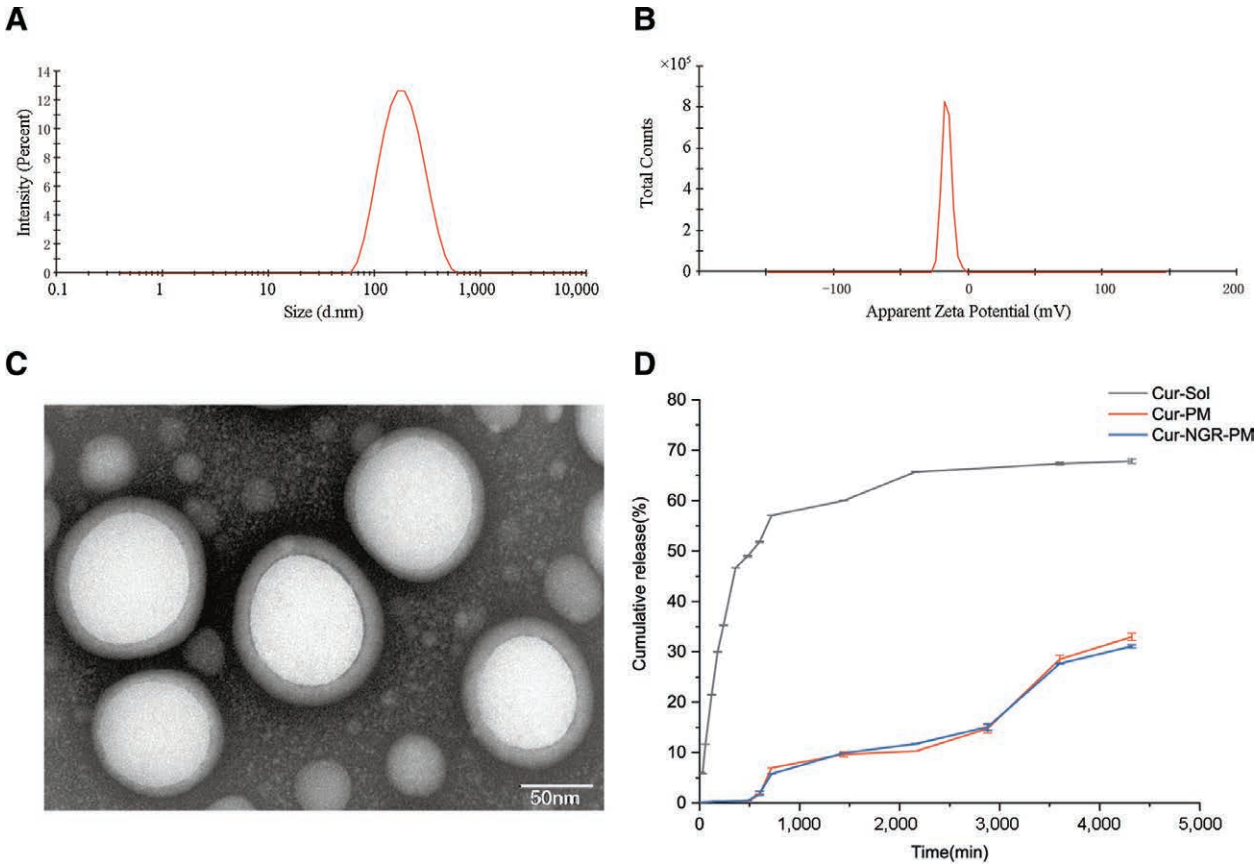

Figure 3. Characterization of the Cur-PM. (A) Micelle size distribution. (B) Zeta potential of polymer micelles. (C) TEM image of Cur-NGR-PM (bar = 50 nm). (D) Release behaviors of Cur from the PM at 37°C (mean ± SD, $n = 3$). Cur: Curcumin; Cur-Sol: Curcumin solution; NGR: Asn–Gly–Arg; PM: Polymer micelles; SD: Standard deviation; TEM: Transmission electron microscopy.

In vitro drug-release profile study

Cur release was time-dependent at pH 7.4. Cur release gradually increased over a prolonged period. It means Cur can be continuously released for a certain period, resulting in long-lasting medicinal effects. As shown in Figure 3D, the initial release of Cur appeared to be greater from Cur-Sol than from Cur-PM and Cur-NGR-PM at 1 hour (~10-fold) post-incubation; however, the Cur release from both Cur-PM and Cur-NGR-PM was similar. These data suggest that the polymeric micelle system may temper Cur's initial release and that unmodified and NGR-modified Cur-loaded PM can release Cur steadily for approximately 72 hours.

Differential scanning calorimetry

DSC is widely used to explore lattice changes in drugs in mixed systems[30–31]. The DSC thermograms of Cur, NGR-PM, and the physical mixtures of Cur and PEG-PLGA, Cur-PM, and Cur-NGR-PM are shown in Figure 4. All signals were exothermic. The DSC thermogram revealed that the melting peak of Cur was 184.96°C, which was also detected in the physical mixture of Cur and PEG-PLGA. However, this melting peak was not observed for PM formation. This indicated that Cur was effectively wrapped and protected in micelles, was stable in the body, and was released to exert its pharmacological effects. Therefore, this study supports using PEG-PLGA micelles as an effective drug carrier system.

In vitro cytotoxicity and cellular uptake

The cytotoxicity of PM and Cur solutions in HepG2 and EA.hy926 cells was determined using the MTT assay (Figure 5). A low Cur concentration (2 μg/mL) did not inhibit cell proliferation, and PM showed no cytotoxicity. However, the rate of cytostasis increased with increasing Cur concentrations. In addition, the modified group exhibited a stronger inhibitory effect on HepG2 cells than did the unmodified and solution groups ($P < 0.001$) (Figure 5A). Co-incubation of cells with Cur-free NGR-PM did not inhibit cell proliferation, and NGR-PM showed no obvious cytotoxicity (Figure 5B). Modified group's EA. hy926 cells exhibited the same inhibitory effect (Figure 5C).

Cou6 is a lipid-soluble fluorescent probe commonly used for fluorescence microscopy imaging and cell labeling[32]. Specifically, Cou6 showed an excitation wavelength of 460 nm and an emission wavelength of 500 nm; furthermore, its high laser conversion rate and stable performance can be quantitatively determined in combination with ultraviolet light or fluorescence detection[33].

PM encapsulating Cou6 (Cou6-PM and Cou6-NGR-PM) were prepared, and their cellular uptake efficiencies were determined by measuring the fluorescence intensity of Cou6. The fluorescence intensities of Cou6-PM and Cou6-NGR-PM were higher than that of free Cou6 at all time points (Figure 6A). Fluorescence intensity of Cou6-NGR-PM was significantly increased, especially after modification by NGR, to 1.29 times that in the free Cou6 group, indicating that the uptake of

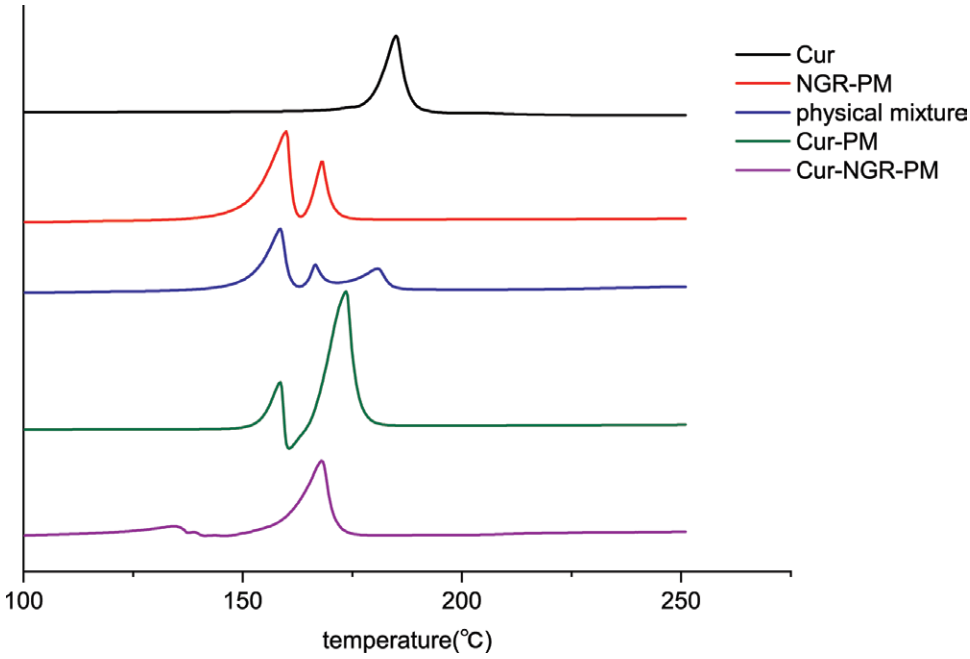

Figure 4. Differential scanning calorimetry of different formulations. Cur: Curcumin; NGR: Asn–Gly–Arg; PM: Polymer micelles.

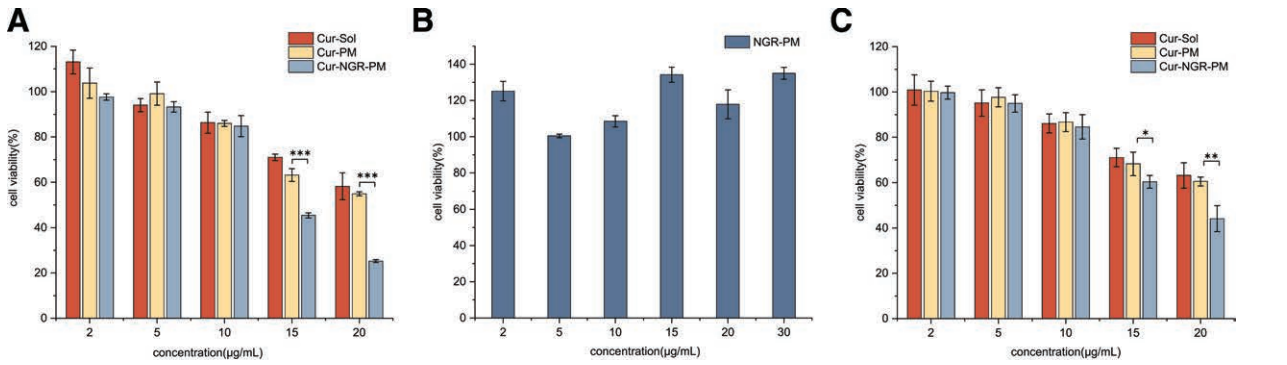

Figure 5. *In vitro* cytotoxicity of different formulations. (A) Cytotoxicity of Cur-Sol, Cur-PM, and Cur-NGR-PM in HepG2 cells. (B) Cytotoxicity of NGR-PM in HepG2 cells. (C) Cytotoxicity of Cur-Sol, Cur-PM, and Cur-NGR-PM in EA.hy926 cells. Data are presented as mean ± SD ($n = 3$). *$P < 0.05$,**$P < 0.01$, ***$P < 0.001$. Cur-Sol: Curcumin solution; NGR: Asn–Gly–Arg; PM: Polymer micelles; SD: Standard deviation.

Cou6 by HepG2 cells was increased by micelle encapsulation and peptide modification (Figure 6B).

The effects of micellar incubation time on cellular uptake profiles were examined using FCM (Figure 6C). Notably, the cellular uptake of micelles by HepG2 cells was time-dependent. Moreover, after incubation for 2 hours, the mean fluorescence intensity and percentage of positive cells increased with increasing micellar incubation time. Importantly, the uptake of Cou6-PM was better than that of the solution group; however, the uptake of Cou6-NGR-PM was better than that of the other groups at 6 hours. Thus, NGR-mediated endocytosis may be the major pathway for micelle entry into HepG2 cells.

In vivo bio-distribution study

In vivo imaging can be used for the real-time dynamic monitoring of cellular activities in small animals. The lipophilic fluorescent dye, Dir, produces infrared fluorescence and can penetrate cells and tissues, making it suitable for *in vivo* tracking. We utilized Dir as a fluorescent probe, incorporated it into the hydrophobic cavity of copolymer micelles, and used *in vivo* imaging to monitor the distribution of micelles in mice. The fluorescence intensity was quantified using a color scale, with red indicating the highest intensity and blue indicating the lowest (Figure 7).

In the saline group treated the tumors of mice, no significant fluorescence changes were observed at the tumor site (Figure 7A). This is because the saline group did not have a significant therapeutic effect on the tumor, or the fluorescently labeled cells did not accumulate at the tumor site. The Dir-Sol group showed no obvious fluorescence after 12 hours, whereas fluorescence was still observed in the PMs groups, indicating that the micelles could achieve prolonged circulation *in vivo*, thus reducing the drug clearance rate and prolonging the *in vivo* residence time. However, the fluorescence intensity at the tumor site gradually increased after 12 hours in the Dir-PM and Dir-NGR-PM groups (Figure 7B), indicating that the drug was delivered and accumulated at the tumor sites *via* micelles. Furthermore, the fluorescence intensity of Dir-NGR-PM was higher than that of Dir-PM, partly because NGR-mediated endocytosis enhanced the targeted delivery to tumor sites (Figure 7C) ($P < 0.05$). These findings suggest that NGR peptide modification is

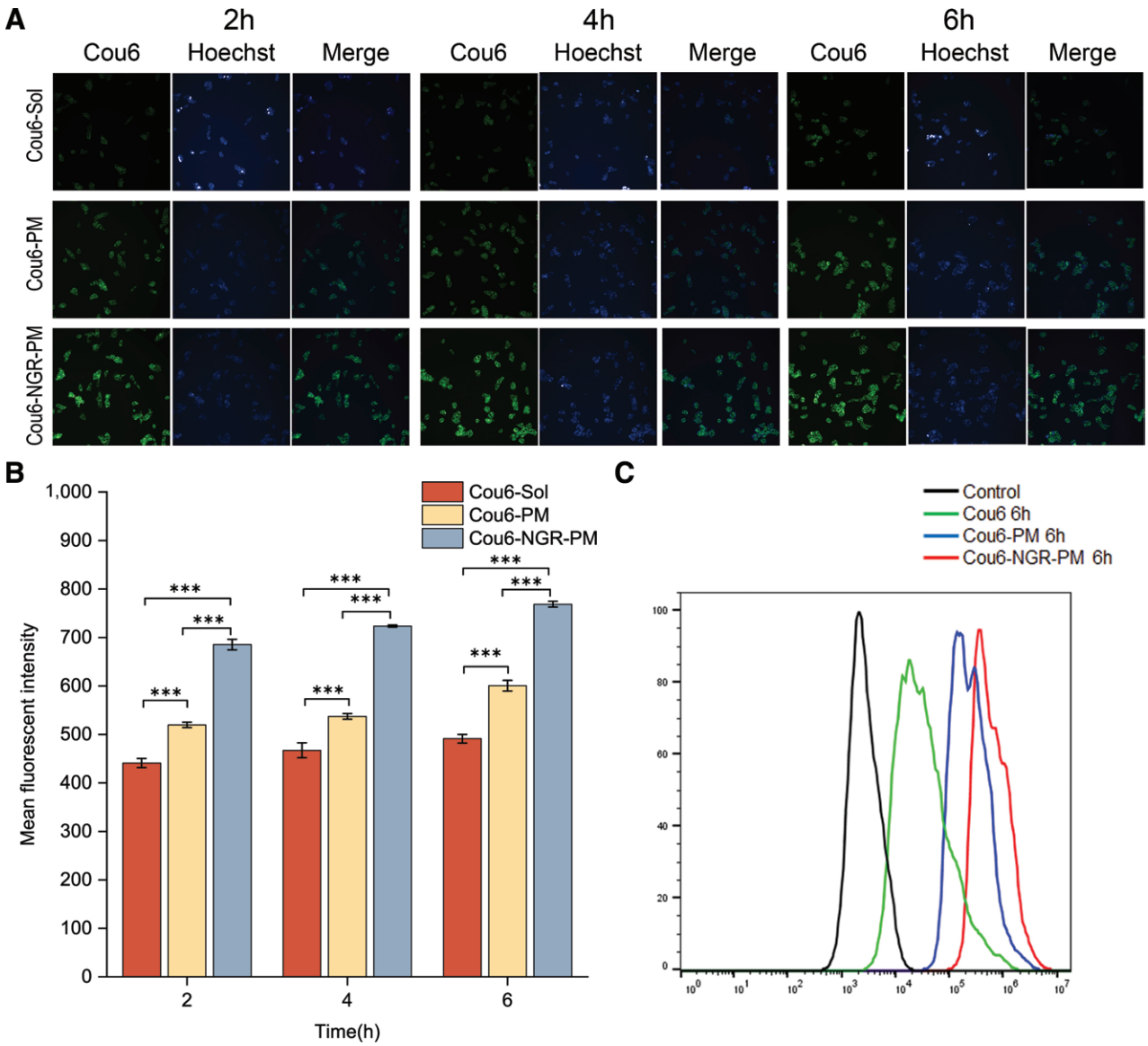

Figure 6. *In vitro* cellular uptake of different formulations in HepG2 cells. (A) The image of cell uptake. (B) The fluorescence intensity of Cou6-labeled PM and NGR-modified Cou6-labeled PM at different incubation times. Data are presented as mean ± SD. ($n = 3$). ***$P < 0.001$. (C) FCM image of HepG2 cells incubated PM. Cou6: Coumarin 6; Cur-Sol: Curcumin solution; FCM: Flow cytometry; NGR: Asn–Gly–Arg; PM: Polymer micelles; SD: standard deviation.

a promising strategy for enhancing drug-loaded micelles' tumor-targeting ability and therapeutic efficacy.

In vivo anti-tumor effect

Xenografted hepatic cancer tumor models were used to investigate the effects of Cur and different PM formulations on tumor growth[34]. Mice were randomly divided into five groups: saline, Cur-Sol, NGR-PM, Cur-PM, and Cur-NGR-PM. H22 cells were injected into the forelimb armpits of mice. When the tumors reached 100 mm^3, the mice in each group were administered Cur (10 mg/kg every 2 days) *via* tail vein injection. The mice were sacrificed 12 days after administration, the tumors were removed and weighed, and the TGI ratio was calculated (Figure 8).

NGR peptides have a neovascular-targeting effect and are thus expected to achieve better tumor treatment outcomes. The effects of the different preparations on tumor volume were investigated (Figure 8A, B). Tumor growth was rapid in the saline and blank micelle groups but was inhibited to varying degrees in the Cur-Sol and PMs groups. Moreover, tumor volumes were significantly smaller ($P < 0.05$) in the Cur-PM and Cur-NGR-PM groups than in the Cur-Sol group. Specifically, the tumor volume was the smallest in the Cur-NGR-PM group, suggesting that the nanocarrier enhanced the anti-tumor effect of Cur. The TGIs of NGR-PM, Cur-Sol, Cur-PM, and Cur-NGR-PM were 6.59%, 29.63%, 45.16%, and 61.58%, respectively (Figure 8C). The TGI in the targeted PM group was higher and showed stronger anti-tumor activity than did those in the solution and non-targeted PM groups. Furthermore, the tumor weight was relatively low, the tumor weight inhibition rate was high in the modification group, and the TIRs of NGR-PM, Cur-Sol, Cur-PM, and Cur-NGR-PM were 13.74%, 34.35%, 48.09%, and 70.99%, respectively (Figure 8D, E). The antitumor activity of Cur-NGR-PM after peptide modification was higher than that of Cur-PM, which is consistent with the above results.

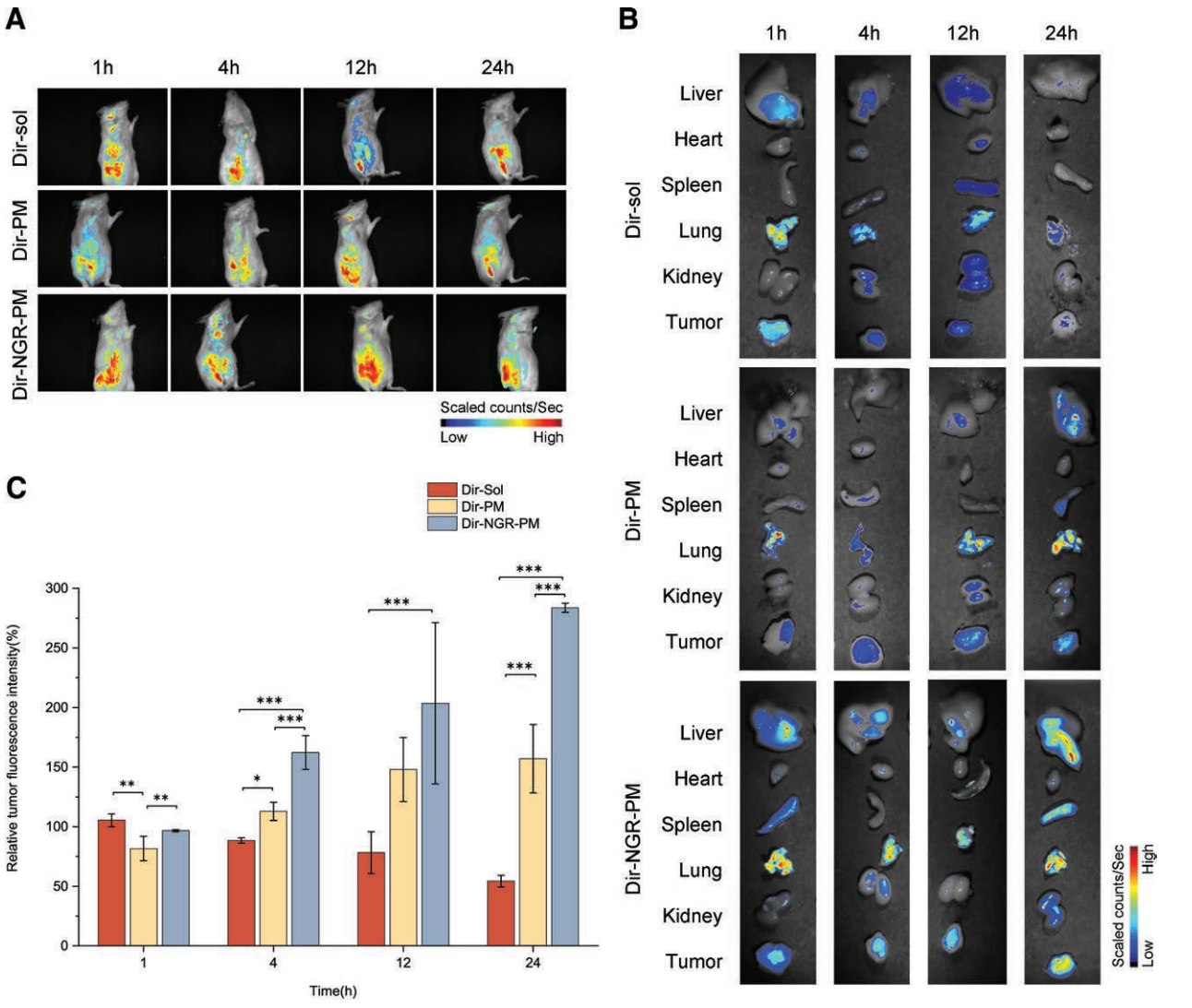

Figure 7. *In vivo* bio-distribution study of different formulations. (A) Tumor fluorescence intensity in tumor-bearing mice after administration. (B) The pictures of the tumors and organs removed from mice. (C) Fluorescence signal of tumor obtained from mice treated with different Dir formulations. Data are presented as mean ± SD. ($n = 3$). *$P < 0.05$,**$P < 0.01$, ***$P < 0.001$. Dir: Dir iodide; NGR: Asn–Gly–Arg; PM: Polymer micelles; SD: Standard deviation; Sol: Solution.

Changes in body weight after drug administration to mice are commonly used as safety indicators. We recorded body weight and calculated the weight suppression rate (IRBW %) in different groups of mice. There were no significant changes in body weight during treatment in the saline, NGR-PM, Cur-Sol, Cur-PM, and Cur-NGR-PM groups (Figure 8F), and the IRBWs values were 13.32%, 7.31%, 6.27%, 8.34%, and 8.43%, respectively (Figure 8G). These results indicated that the preparation had a good safety profile and did not affect mouse growth. The organ index was calculated to investigate the effects of the preparations on specific organs. There was no significant difference between the groups ($P > 0.05$), and the nanocarriers did not increase their distribution in the main organs (Figure 8H). These results indicated that the NGR-mediated PM delivery system was safe and efficient.

Serum alanine transaminase (ALT), aspartate transaminase (AST), and CRE levels were measured to detect hepatic or renal toxicity. Detection was performed using a multifunctional enzyme labeling instrument (TECAN, Basel-City, Switzerland) according to the manufacturer's specifications. ALT is mainly present in the cytoplasm of hepatocytes, while AST is mainly present in the cytoplasm and mitochondria of hepatocytes, and are released into the systemic circulation following hepatocyte damage, increasing serum ALT and AST activity. Thus, monitoring serum ALT and AST levels can be used to evaluate hepatocyte damage[35]. The serum ALT and AST levels increased sequentially in the Cur-NGR-PM, Cur-PM, Cur-Sol, and saline groups. The Cur-NGR-PM group had the lowest level and was statistically significant compared with the other groups ($P < 0.001$), suggesting that Cur-NGR-PM may have a hepatoprotective effect (Figure 8I, J)[36]. Circulating serum levels of free CRE depend entirely on its excretion rate; therefore, serum CRE levels can be used to evaluate glomerular filtration rate and renal function. Furthermore, serum CRE levels were significantly lower in the Cur-NGR-PM group than those in the saline, Cur-Sol, and Cur-PM groups ($P < 0.01$), indicating that Cur-NGR-PM reduced liver and kidney damage (Figure 8K).

Microscopic changes in mouse organs were observed histologically using H&E staining to assess the toxicity of the different preparations (Figure 9). Liver tissues in the saline, NGR-PM, and Cur-Sol groups showed few

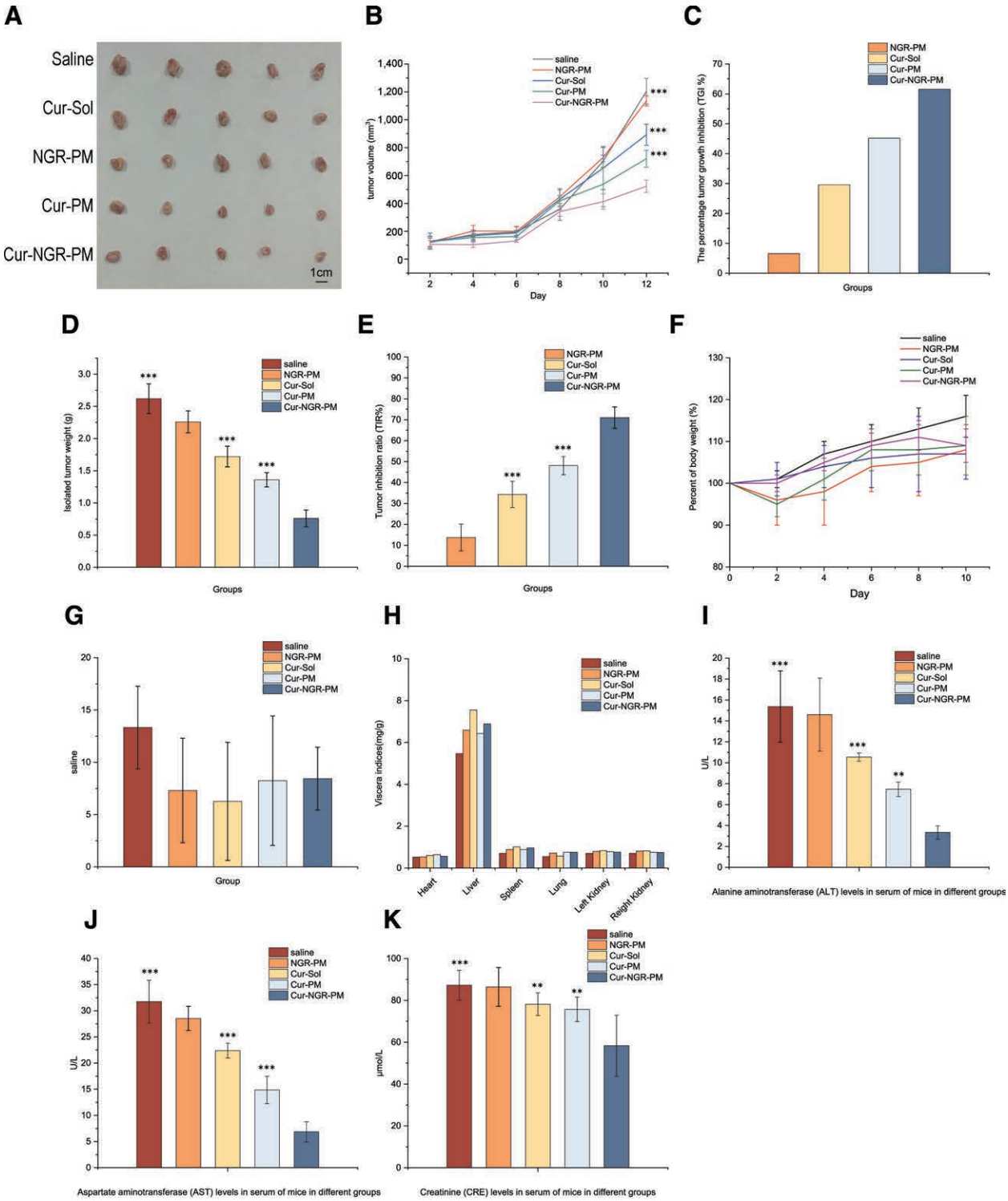

Figure 8. *In vivo* antitumor effect. (A) Tumor tissues. (B) The volume-time change of tumor. (C) TGI rate. (D) The tumor tissue weight of mice. (E) The TIR of mice. (F) The relative weight-time change of mice. (G) The IRBW of mice. (H) The organ index of mice. (I) ALT levels in the serum of mice. (J) AST levels in the serum of mice. (K) CRE levels in the serum of mice. Data are presented as mean ± SD. ($n = 5$). ***$P < 0.001$ versus Cur-NGR-PM, **$P < 0.01$ versus Cur-NGR-PM. ALT: Alanine aminotransferase; AST: Aspartate aminotransferase; CRE: Creatinine; Cur: Curcumin; IRBW: Inhibition rate of body weight; NGR: Asn–Gly–Arg; PM: Polymer micelles; SD: Standard deviation; Sol: Solution; TGI: Tumor growth inhibition; TIR: Tumor inhibition rate.

fatty lesions, nuclear constrictions, deep staining, and a small increase in the number of inflammatory cells. There were minor changes in the structural morphology of the renal tubules and glomeruli in the normal saline, NGR-PM, and Cur-Sol groups and slight reductions in glomeruli and inflammatory cell infiltration. There were no significant changes in visceral tissue morphology in the Cur-PM and Cur-NGR-PM groups, indicating that the mice tolerated PM with no obvious systemic toxicity.

MVD assay

CD31 is a sensitive and specific endothelial marker. Therefore, we stained the tumor blood vessels with

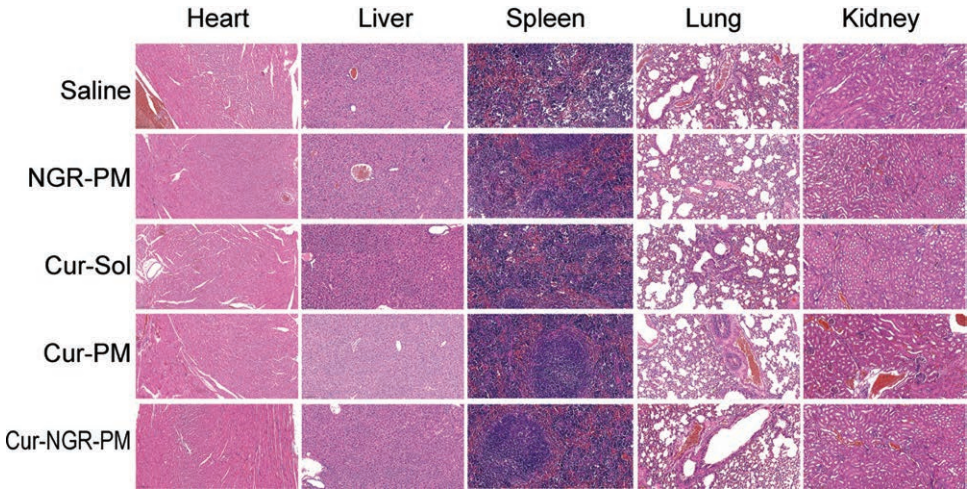

Figure 9. HE staining analysis morphological of visceral tissues. Cur: Curcumin; H&E: Hematoxylin–eosin; NGR: Asn–Gly–Arg; PM: Polymer micelles.

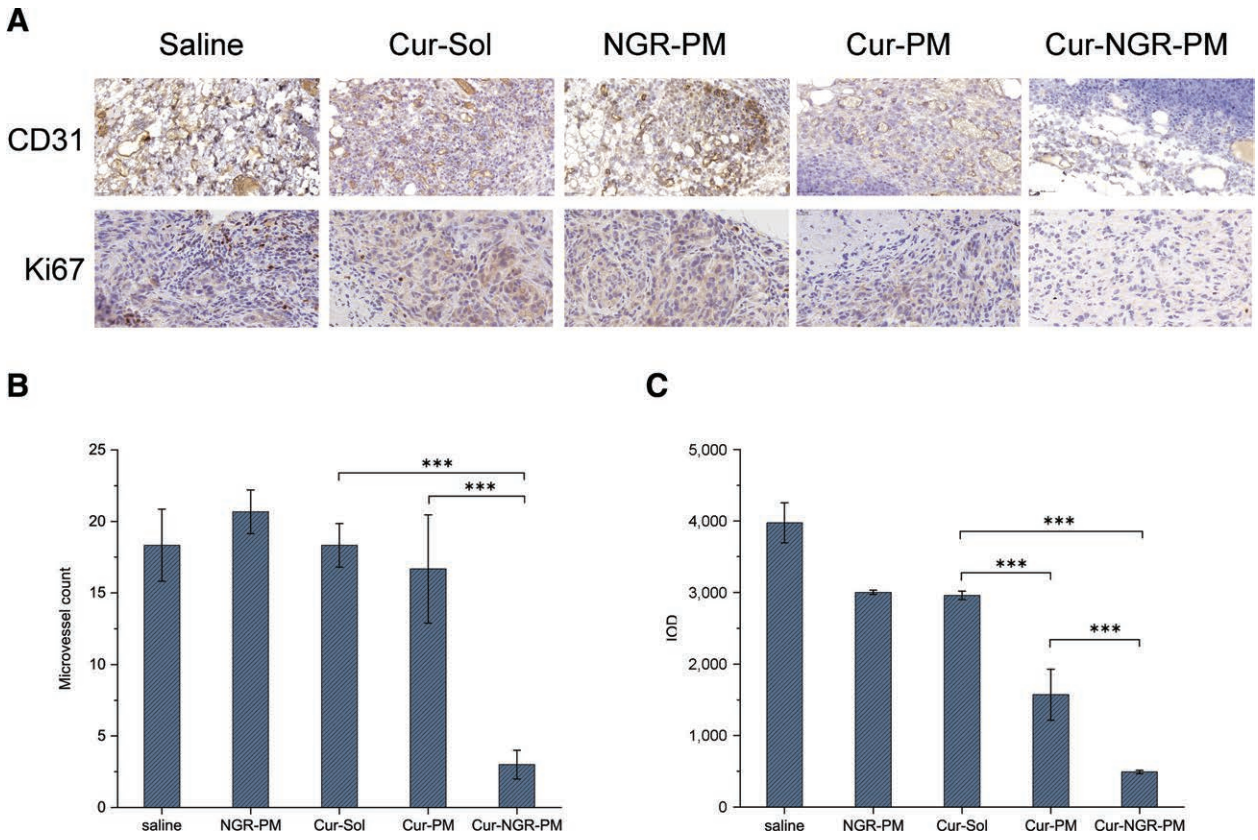

Figure 10. MVD assay. (A) CD31 and Ki67 analyses of excised tumors after the last treatments. For all images, the magnification is 400×. (B) MVD determination by immunohistochemistry on formaldehyde-fixed tumors. (C) IOD determination. Data are presented as mean ± SD. ($n = 5$). ***$P < 0.001$. Cur: Curcumin; IOD: Cumulative optical density; MVD, Microvascular density; NGR: Asn–Gly–Arg; PM: Polymer micelles; SD: Standard deviation; Sol: Solution.

anti-CD31 antibodies to determine whether the anti-tumor effects of the different preparations were related to their anti-angiogenic effects. Numerous CD31-positive cells were detected in the normal saline, NGR-PM, and Cur-PM groups. However, the number was significantly reduced in the Cur-NGR-PM group (Figure 10A), and the effect of Cur-PM treatment was significantly improved after NGR modification.

The proliferation of tumor cells *in vivo* was detected using immunohistochemical staining. Ki67 expression levels were significantly lower in the NGR-modified PM group than in the other groups (Figure 10A), indicating that Cur-NGR-PM had a weaker inhibitory effect than the other preparations. Furthermore, Cur-NGR-PM showed good anti-proliferative activity, and NGR showed good recognition and penetration abilities in tumor cells.

MVD was detected by immunohistochemistry. MVD was significantly reduced in the Cur-NGR-PM group (3.0 ± 1.0) compared with the Cur-PM (16.7 ± 3.8) and Cur groups (18.3 ± 1.5) ($P < 0.001$) (Figure 10B). At the same time, there was no significant difference between the unmodified and solution groups, suggesting that

NGR targeted the vascular system and enhanced the antitumor effect of Cur.

A positive cumulative optical density (IOD) confirmed that NGR-targeted tumor neovascularization *in vivo* (Figure 10C). Images were obtained from three random fields in each tissue slice for each group, and the cumulative IOD of each image was determined using Image-Pro Plus 6.0 software. The results showed that NGR-targeted vascular effects increased drug specificity in tumors.

Discussion

Angiogenesis, the formation of new blood vessels from the pre-existing vasculature, is the rate-limiting step in solid tumor growth. CD13 (an APN, a cell-surface antigen) is a critical regulator of angiogenesis[37]. It is expressed in many cell types, including white blood, endothelial, and liver cells. In tumor cells, CD13 expression levels are usually higher than those in normal cells and are associated with tumor invasion and metastasis[38]. The main role of CD13 in tumor cells is to participate in the degradation of the extracellular matrix and the invasion of tissues. Furthermore, CD13 can break down matrix proteins such as collagen and fibronectin, thereby promoting the invasion and metastasis of tumor cells. In addition, CD13 can interact with other molecules, such as CD44 and integrin, to promote tumor growth. Therefore, inhibition of CD13 expression or activity may be an effective strategy for tumor treatment. NGR, which recognizes a tumor-specific isoform of CD13, has been identified as a potent tumor-targeting ligand[19]. NGR peptides target tumor vasculature *via* interactions with CD13. Our study validated this treatment option. Unlike Cur-Sol and Cur-PM, anti-angiogenic therapy using Cur-NGR-PM showed potent antitumor activity in *in vitro* cell experiments and H22-bearing animal models. Therefore, we believe that NGR peptide-modified micelles can bind to or target angiogenic blood vessels.

In conclusion, in this study, NGR-PEG-PLGA was prepared and demonstrated excellent HepG2 cell-specific targeting of Cur to liver cancer cells. Cur-NGR-PM was significantly superior to traditional micelles in inhibiting tumor growth and angiogenesis, suggesting that Cur-NGR-PM is a promising anticancer agent. The polymeric micelles prepared in this study had a size of about 140 to 150 nm and a slight negative charge (−12 to −15 mV). The characterization study indicated that NGR modification did not alter the particle size, zeta potential, or Cur EE compared with Cur-PM. HepG2 cells were used to evaluate the *in vitro* targeting properties of NGR toward tumor cells. Moreover, NGR-modified carriers have been reported to increase drug uptake by APN/CD31-positive cells *via* APN/CD31 receptor-mediated endocytosis. Our results demonstrated that the NGR-modified micelles specifically targeted HepG2 and EA.hy926 cells, indicating that these modified micelles enhanced cellular drug uptake. Both quantitative and qualitative results suggested an essential role for NGR modification in cellular uptake and provided strong evidence for the anti-neovascularization effect of NGR in cells. *In vivo* imaging studies indicated that Dir-NGR-PM has targeting and penetration abilities for pathological angiogenesis in H22 tumor-bearing mice. Dir-NGR-PM had a longer effect in mice, and ex *vivo* tumor tissue fluorescence showed stronger tumor targeting, which was related to NGR peptide-mediated endocytosis. The *in vivo* anti-tumor studies indicated that Cur-NGR-PM had significantly greater anti-tumor efficacy than did Cur-PM in H22 tumor-bearing mice. In addition, the immunohistochemical analysis indicated that the *in vivo* anti-angiogenic effect of Cur-NGR-PM was significantly higher than that of Cur-Sol or Cur-PM. However, the study is still incomplete due to a lack of *in vitro* anti-angiogenic activity experiments, which may highlight the superiority of NGR-PM in inhibiting neovascularization. Here, we used a liver cancer model that cannot represent all situations, as different tumors have different responses to angiogenesis inhibition. In our future studies, we will attempt to solve this problem. In summary, Cur-NGR-PM prepared in this study showed improved anti-angiogenic and anti-tumor activity *in vitro* and *in vivo* and may have potential applications in hepatic carcinoma therapy.

Conflicts of interest statement

The authors declare no conflict of interest.

Funding

This study was supported by Scientific Research Project of Tianjin Municipal Education Commission (No. 2019KJ080).

Author contributions

Rui Liu and Pan Guo participated in research design and writing of the paper. Zhongyan Liu, Changxiang Yu, Ying Zhang, Xiaojiao Feng, Qingqing Zhang, Wenli Dang, Xintao Jia, Bei Jia, Jiachen He, Ziwei Li, Huihui Li, Xueli Guo, and Pan Guo participated in the performance of the research. Dereje Kebebe, Jiaxin Pi, and Pan Guo contributed new reagents or analytic tools. Bin Xing, Changxiang Yu, Ying Zhang, and Pan Guo participated in data analysis.

Ethical approval of studies and informed consent

The protocols and any amendments or procedures involved in the care or use of animals in the study were in compliance with the regulations for animal experimentation issued by the State Committee of Science and Technology of China and approved by TJUTCM's Institutional Animal Care and Use Committee (Document number TCM-LAEC2022128).

Acknowledgments

We acknowledge the help of Gina F, who kindly improved the language of the paper.

Data availability statement

The datasets generated during and/or analyzed during the current study are available from the corresponding author on reasonable request.

References

[1] Mahtabifard A, Merritt RE, Yamada RE, et al. *In vivo* gene transfer of pigment epithelium-derived factor inhibits tumor growth in syngeneic murine models of thoracic malignancies. *J Thorac Cardiovasc Surg* 2003;126(1):28–38.

[2] Shim JS, Kim JH, Cho HY, et al. Irreversible inhibition of CD13/aminopeptidase N by the antiangiogenic agent curcumin. *Chem Biol* 2003;10(8):695–704.

[3] Su L, Cao J, Jia Y, et al. Development of synthetic aminopeptidase N/CD13 inhibitors to overcome cancer metastasis and angiogenesis. *ACS Med Chem Lett* 2012;3(12):959–964.

[4] Morgan R, Endres J, Behbahani-Nejad N, et al. Expression and function of aminopeptidase N/CD13 produced by fibroblast-like synoviocytes in rheumatoid arthritis: role of CD13 in chemotaxis of cytokine-activated T cells independent of enzymatic activity. *Arthritis Rheumatol* 2015;67(1):74–85.

[5] Licona-Limon I, Garay-Canales CA, Munoz-Paleta O, et al. CD13 mediates phagocytosis in human monocytic cells. *J Leukoc Biol* 2015;98(1):85–98.

[6] Liang W, Gao B, Xu G, et al. Possible contribution of aminopeptidase N (APN/CD13) to migration and invasion of human osteosarcoma cell lines. *Int J Oncol* 2014;45(6):2475–2485.

[7] Pulido-Moran M, Moreno-Fernandez J, Ramirez-Tortosa C, et al. Curcumin and health. *Molecules* 2016;21(3):264.

[8] Shanmugam MK, Rane G, Kanchi MM, et al. The multifaceted role of curcumin in cancer prevention and treatment. *Molecules* 2015;20(2):2728–2769.

[9] Tomeh MA, Hadianamrei R, Zhao X. A Review of curcumin and its derivatives as anticancer agents. *Int J Mol Sci* 2019;20(5):1033.

[10] Wang M, Jiang S, Zhou L, et al. Potential mechanisms of action of curcumin for cancer prevention: focus on cellular signaling pathways and miRNAs. *Int J Biol Sci* 2019;15(6):1200–1214.

[11] Wang J, Wang C, Bu G. Curcumin inhibits the growth of liver cancer stem cells through the phosphatidylinositol 3-kinase/protein kinase B/mammalian target of rapamycin signaling pathway. *Exp Ther Med* 2018;15(4):3650–3658.

[12] Pan Z, Zhuang J, Ji C, et al. Curcumin inhibits hepatocellular carcinoma growth by targeting VEGF expression. *Oncol Lett* 2018;15(4):4821–4826.

[13] Lu Y, Wang J, Liu L, et al. Curcumin increases the sensitivity of paclitaxel-resistant NSCLC cells to paclitaxel through microRNA-30c-mediated MTA1 reduction. *Tumour Biol* 2017;39(4):1010428317698353.

[14] Menon VP, Sudheer AR. Antioxidant and anti-inflammatory properties of curcumin. *Adv Exp Med Biol* 2007;595:105–125.

[15] Kumar S, Fayaz F, Pottoo FH, et al. Nanophytomedicine based novel therapeutic strategies in liver cancer. *Curr Top Med Chem* 2020;20(22):1999–2024.

[16] Pachauri M, Gupta ED, Ghosh PC. Piperine loaded PEG-PLGA nanoparticles: preparation, characterization and targeted delivery for adjuvant breast cancer chemotherapy. *J Drug Delivery Sci Technol* 2015;29:269–282.

[17] Yang Y, Zhang J, Zou H, et al. Synthesis and evaluation of (68)Ga-labeled dimeric cNGR peptide for PET imaging of CD13 expression with ovarian cancer xenograft. *J Cancer* 2021;12(1):244–252.

[18] Liu C, Qi W, Teng Z, et al. NGR-modified PEG-PLGA micelles containing Shikonin enhance targeting of dendritic cells for therapy of allergic rhinitis. *Int Immunopharmacol* 2022;107:108649.

[19] Wang X, Wang Y, Chen X, et al. NGR-modified micelles enhance their interaction with CD13-overexpressing tumor and endothelial cells. *J Control Release* 2009;139(1):56–62.

[20] Zhao BJ, Ke XY, Huang Y, et al. The antiangiogenic efficacy of NGR-modified PEG-DSPE micelles containing paclitaxel (NGR-M-PTX) for the treatment of glioma in rats. *J Drug Target* 2011;19(5):382–390.

[21] Jiao Z, Liu N, Chen Z. Selection suitable solvents to prepare paclitaxel-loaded micelles by solvent evaporation method. *Pharm Dev Technol* 2012;17(2):164–169.

[22] Perumal S, Atchudan R, Lee W. A review of polymeric micelles and their applications. *Polymers* 2022;14(12):2510.

[23] Lv Y, He H, Qi J, et al. Visual validation of the measurement of entrapment efficiency of drug nanocarriers. *Int J Pharm* 2018;547(1–2):395–403.

[24] Xie X, Tao Q, Zou Y, et al. PLGA nanoparticles improve the oral bioavailability of curcumin in rats: characterizations and mechanisms. *J Agric Food Chem* 2011;59(17):9280–9289.

[25] Qiao JB, Fan QQ, Xing L, et al. Vitamin A-decorated biocompatible micelles for chemogene therapy of liver fibrosis. *J Control Release* 2018;283:113–125.

[26] Qi X, Gao C, Yin C, et al. Development of quercetin-loaded PVCL-PVA-PEG micelles and application in inhibiting tumor angiogenesis through the PI3K/Akt/VEGF pathway. *Toxicol Appl Pharmacol* 2022;437:115889.

[27] Song Z, Feng R, Sun M, et al. Curcumin-loaded PLGA-PEG-PLGA triblock copolymeric micelles: preparation, pharmacokinetics and distribution *in vivo*. *J Colloid Interface Sci* 2011;354(1):116–123.

[28] Gu Z, Chang M, Fan Y, et al. NGR-modified pH-sensitive liposomes for controlled release and tumor target delivery of docetaxel. *Colloids Surf B* 2017;160:395–405.

[29] Zhang K, Tang X, Zhang J, et al. PEG-PLGA copolymers: their structure and structure-influenced drug delivery applications. *J Control Release* 2014;183:77–86.

[30] Agrawal Y, Petkar KC, Sawant KK. Development, evaluation and clinical studies of Acitretin loaded nanostructured lipid carriers for topical treatment of psoriasis. *Int J Pharm* 2010;401(1-2):93–102.

[31] Gao F, Chen Z, Zhou L, et al. Preparation, characterization and in vitro study of bellidifolin nano-micelles. *RSC Adv* 2022;12(34):21982–21989.

[32] Ashour AA, El-Kamel AH, Mehanna RA, et al. Luteolin-loaded exosomes derived from bone marrow mesenchymal stem cells: a promising therapy for liver fibrosis. *Drug Deliv* 2022;29(1):3270–3280.

[33] Ding Y, Cui W, Sun D, et al. *In vivo* study of doxorubicin-loaded cell-penetrating peptide-modified pH-sensitive liposomes: biocompatibility, bio-distribution, and pharmacodynamics in BALB/c nude mice bearing human breast tumors. *Drug Des Devel Ther* 2017;11:3105–3117.

[34] Zhou Z, Li L, Yang Y, et al. Tumor targeting by pH-sensitive, biodegradable, cross-linked N-(2-hydroxypropyl) methacrylamide copolymer micelles. *Biomaterials* 2014;35(24):6622–6635.

[35] Yuan R, Tao X, Liang S, et al. Protective effect of acidic polysaccharide from Schisandra chinensis on acute ethanol-induced liver injury through reducing CYP2E1-dependent oxidative stress. *Biomed Pharmacother* 2018;99:537–542.

[36] Chen W, Luo Y, Liu L, et al. Cryptotanshinone inhibits cancer cell proliferation by suppressing mammalian target of rapamycin-mediated cyclin D1 expression and Rb phosphorylation. *Cancer Prev Res (Phila)* 2010;3(8):1015–1025.

[37] Zou M, Zhang L, Xie Y, et al. NGR-based strategies for targeting delivery of chemotherapeutics to tumor vasculature. *Anticancer Agents Med Chem* 2012;12(3):239–246.

[38] Saiki I, Fujii H, Yoneda J, et al. Role of aminopeptidase N (CD13) in tumor-cell invasion and extracellular matrix degradation. *Int J Cancer* 1993;22(1):137–143.

How to cite this article: Liu R, Liu ZY, Guo XL, Kebebe D, Pi JX, Guo P. Construction of curcumin-loaded micelles and evaluation of the antitumor effect based on angiogenesis. Acupunct Herb Med 2023;3(4):343–356. doi: 10.1097/HM9.0000000000000079